

On the origin of chains of cavities in the rotating flow between cylinders

© E.L. Amromin

Federal Way WA 98003, USA
 e-mail: Amromin@aol.com

Received April 25, 2021

Revised June 14, 2021

Accepted July 4, 2021

Cavitation between rotating and immobile cylinders appears in the form of a regular chain of bubbles. The bubble sizes are practically equal, as well as the distances between the bubbles and their azimuthal locations. Though such a form of cavitation has been observed in numerous experiments (in particular, in the experiments with bearings), its nature was not clarified. The presented analysis shows that breakdown of the flow axial symmetry due to displacement of the axis of one of cylinders leads to the regular wave-similar three-dimensional flow perturbations. Their „wavelength“ is predetermined by the minimal gap between cylinders. Though the flow between cylinders is not curl-free, these perturbations can be determined with the use of a velocity potential.

Keywords: Cavitation, circular cylinders, misaligned cylinders, non-viscous flow.

DOI: 10.21883/TP.2022.14.55216.119-21

Introduction

The present work is devoted to the experiment [1] in which a periodic chain of bubbles was found, which appear in a flow between non-coaxial cylinders. This periodicity is not explained. Periodic incipient cavitation patches have also been reported in studies [1–8] and reviews [9,10] concerning flows in bearings. Such bubbles appear just below the line of minimum clearance between the cylinders. Analytical studies explaining the existence of such formations are in the literature not found.

Thus, the flow between two circular cylinders with parallel axes is analyzed here. The flow diagram in Fig. 1 corresponds to the experiment [1]. The outer cylinder of radius R rotates with frequency Ω , (R will be used below as the unit of length, ΩR will be used as the unit of velocity). The radius of the inner stationary cylinder is equal to R_i . One of the axes of the cylinder coincides with the axis z . The other is at a distance \hat{y} below the first. The Y-axis runs along the minimum clearance between

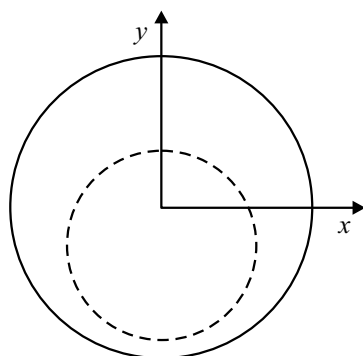


Figure 1. View of the cross section of the flow $z = \text{const}$; the solid circle shows the sections of the rotating cylinder, the dotted line shows the stationary cylinder.

the cylinders. Experimental data [1] refer to outer cylinder of radius 0.025 m, rotating with frequencies in the range $0.03 < \Omega < 0.34 \text{ s}^{-1}$.

The traditional mathematical model for flow between cylinders is based on considering the Reynolds equation for hydrodynamic lubrication, but this equation depends on only two variables. Meanwhile, the occurrence of a clearance between the axes of the cylinders leads to the transformation of the axisymmetric flow into the three-dimensional one, and it becomes necessary to take into account three-dimensional perturbations of the flow. Although the unperturbed flow is not curl-free, its perturbations can be determined using velocity potentials, as described in [11,12] for other flows with visible regular structure.

1. Inviscid flow calculation

Let's consider the flow between non-coaxial cylinders as the perturbed steady flow between coaxial cylinders. Two cylindrical coordinate systems will be used. The system $\{z, r, \theta\}$ is connected with the outer cylinder, the system $\{z, r^*, \varphi\}$ is connected with the inner cylinder; θ and φ are measured from the symmetry line of the section. The unperturbed flow can be described by the approximate formula

$$u_0\{r, \theta\} = \left(r - \frac{\varepsilon^2}{r}\right) \frac{1 - R_i^2(1 - 2 \ln R_i)}{1 - \varepsilon^2 + 2\varepsilon^2 \ln \varepsilon} \quad (1)$$

for the circumferential velocity in the flow between the cylinders, where $\varepsilon(\theta) = 1 - h(\theta)$, h is distance (clearance) between the surfaces of the cylinders. This formula satisfies the law of conservation of mass. The fluid flow through the sections $\theta = \text{const}$ between the coaxial cylinders is $0.5[1 - R_i^2(1 - 2 \ln R_i)]/(1 - R_i^2)$. Equation (1) assumes that the same flow will be maintained after the displacement of the axis of the outer cylinder, and the similarity of

the velocity profile along the radius continuation of inner cylinder will also be preserved. The value h is measured along this continuation. It is also possible to find from equation (1) the velocity of the unperturbed flow on the surfaces of the inner cylinder, which is equal to zero. On the outer cylinder, it grows with the decrease of h .

A three-dimensional velocity perturbation can be defined using the velocity potential Φ , which consists of two components, which are solutions of the Laplace's equation (to which the same law leads for incompressible liquids comes). First component

$$\Phi_1 = A \sin(\theta) \cos(kz) I_1(kr), \tag{2}$$

where I_1 is the modified Bessel function, is the fundamental solution [13] of the Laplace's equation; the wavenumber k is found from the condition

$$\frac{dI_1}{dr}(k) = 0. \tag{3}$$

Equation (3) has many roots. The choice between them must be made taking into account the additional condition $\frac{dI_1}{dr}(k - kH) \simeq 0$. Here H is minimum clearance between cylinders. Second component

$$\Phi_2 = \frac{1}{4\pi} \iiint_{S_0+S_i}^{\square} \frac{Q ds}{D} \tag{4}$$

is determined using intensity sources or sinks Q distributed over the surfaces of both cylinders. Here S_0 and S_i are surfaces of outer and inner cylinders, distance $D = \sqrt{(z - \xi)^2 + (\sin \theta - R_i \sin \varepsilon)^2 + (\cos \theta - R_i \cos \varphi - \hat{y} \cos \varphi)^2}$. The boundary conditions for determining the intensity Q are the impermeability conditions for both surfaces. This condition has the form

$$\frac{\partial \Phi_2}{\partial r} + \frac{\partial \Phi_1}{\partial r} = 0 \tag{5}$$

on S_0 , while on S_i

$$\frac{\partial \Phi_2}{\partial r^*} + \frac{\partial \Phi_1}{\partial r^*} + u_0 \cos(\widehat{r, \theta}) = 0. \tag{6}$$

Additional condition

$$\iiint_{S_0}^{\square} \left[\frac{\partial \Phi_1}{\partial r} + \frac{1}{4\pi} \frac{\partial}{\partial r} \iiint_{S_i}^{\square} \frac{Q ds}{D} \right] ds = 0 \tag{7}$$

allows to determine the coefficient A . The solution of this problem for the Laplace equation can be found by the boundary element method. The presence of exact formulas for the coordinates S_0 and S_i makes it possible to avoid the approximation of these surfaces (unlike the algorithm described, for example, in [14]) and thereby reduce calculation errors. After calculating the velocity components, the pressure can be calculated by integrating the Navier–Stokes equation written in cylindrical coordinates (see Appendix 2

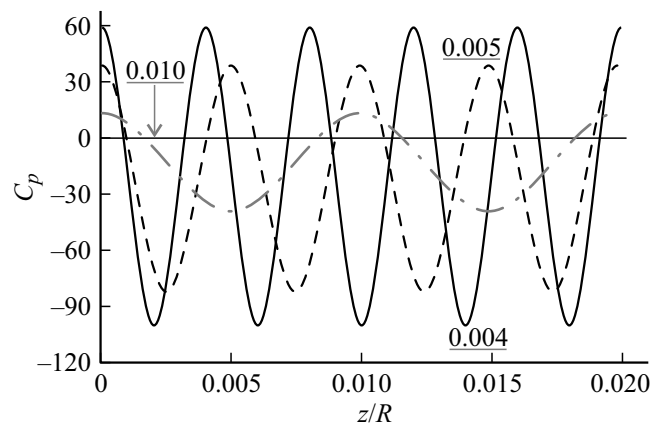


Figure 2. Distribution of pressure along the line of the minimum clearance between the cylinders for $R_i = 0.75R$; the numbers near the curves show the values H ; the pressure coefficient is normalized to $0.5\rho(\Omega R)^2$.

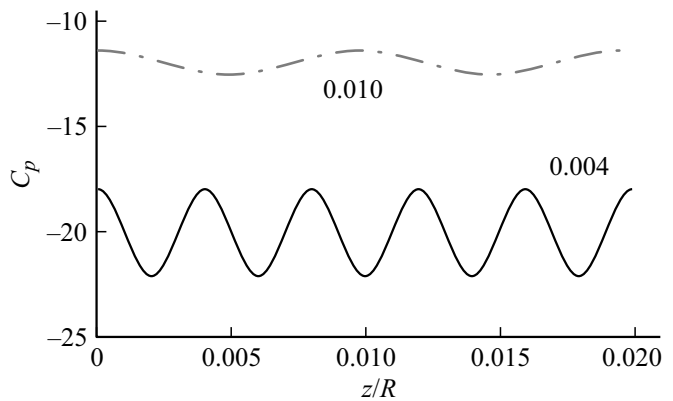


Figure 3. Distribution of pressure along the line of the minimum clearance between the cylinders for $R_i = 0.95R$; the numbers near the curves show the values H ; the pressure coefficient is normalized to $0.5\rho(\Omega R)^2$.

in [15]). However, in the minimum clearance between the cylinders, the radial velocity component is negligible, and its azimuthal component has the maximum. Therefore, when integrating, the terms depending on the viscosity can be omitted.

Comparisons of the calculated pressure distribution over the cross sections of the outer cylinders ($z = \text{const}$) for two values R_i and for several ones $H = 1.0 - R_i - \hat{y}$ are shown in Fig. 2 and 3 for the difference between R and R_i , which is much smaller than in the experiment [1], but this is closer to the situation with bearings [9]. As can be seen from these figures, the contribution Φ_1 leads to the axial and radial pressure waves mentioned in [2]. As can be deduced from the above calculations, the constant distance between the two parallel axes of the cylinders results in the generation of „waves“. In the vicinity of pressure minima must take place emerging cavities.

Comparison of the calculated dependences for wavelength λ with those measured in [1] is shown in Fig. 4. Their

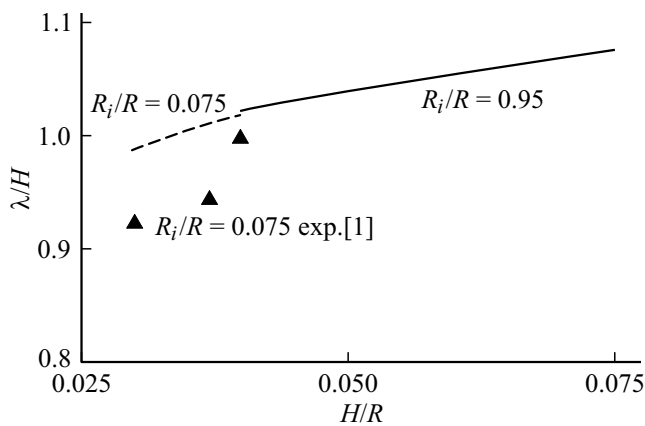


Figure 4. Dependences of wavelengths on the minimum clearances between cylinders. Lines — calculations, triangles — experimental data [1].

difference can be evaluated as satisfactory. The calculated curve for another ratio R_i/R and, accordingly, other \hat{y} on the same diagram (dashed curve) practically coincides with the first one. Thus, the developed mathematical formulation of the problem makes it possible to explain the nature of the observed systems of cavities.

2. On forecast the origin of cavitation

The studied regular cavitation spots appeared in a very wide range of Reynolds numbers, including at sufficiently high Re (at $Re > 10^6$ in [6]). In particular, in the experiments [1] carried out with the PDMS1000 liquid, which has the kinematic viscosity $\nu = 10^{-3} \text{ m}^2\text{s}^{-1}$, corresponding values of Re are below 1.0. To analyze these experiments, the models of viscous fluid cavitation flows used in [16] (but previously proposed in [17]) or in [18] (but previously proposed in [19]) don't match.

Thus, the author compares his results with the experimental data [1] on the occurrence of cavitation, using very approximate estimates. First, he assumed that the cavities appear in the form of spherical bubbles near the points of separation of the laminar boundary layer from the cylinder. Secondly, it was assumed that the pressure in the liquid in these places can be estimated without taking into account the reverse effect of the separation zone on it (as in the outdated method used in [20]). Thirdly, since the known criteria for separation of a laminar boundary layer do not work at such small Re (as well as the special criterion from [10] for flows between cylinders), the point of maximum pressure gradient was chosen as the point of separation of the boundary layer. Nevertheless, the calculations are in good agreement with the experimental data [1]: the point of the gradient maximum is 6.5 degrees below the clearance minimum, while the observed bubbles were located approximately below 7 degrees. Example of the calculated pressure distribution over the cross section of the inner cylinder in an ideal fluid is shown in Fig. 5. The

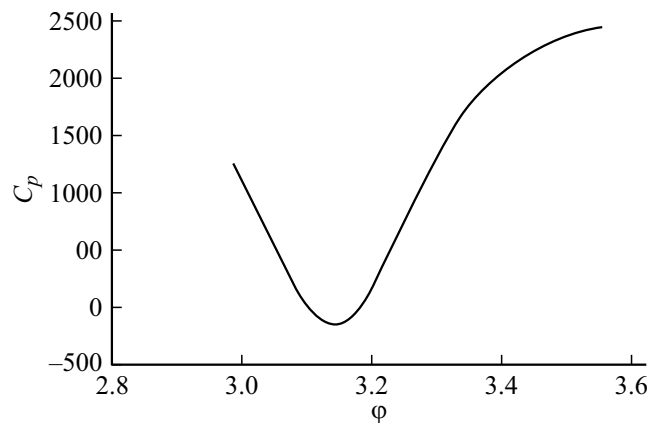


Figure 5. Example of the calculated pressure distribution over the cross section of the inner cylinder ($H = 0.005$); the pressure coefficient is normalized on $0.5\rho(\Omega R)^2$.

cavitation number in [1] was not entered and comparison of cavitation occurrence numbers is not possible.

Thus, the satisfactory solution for the considered type of separated flows was found within the framework of the ideal fluid theory (as well as in the situations considered in [21]). Typically, calculations of internal cavitating flows for very low Reynolds numbers are done using the software for Navier–Stokes equation (as in [22]). There is only one work [23] devoted to cavitation between cylinders at such Re , however, rather fully-developed cavitation was considered there, and there should be a smoothing back effect of the cavity on periodic pressure minima. Thus, it is impossible to compare the results of this work with the results of [23].

Accurate quantitative analysis at Re values corresponding to the data [1] may be possible by the Direct Numerical Simulation (DNS) method. However, the surface tension force must be included in the analysis, since, according to the photo [1], for $H = 0.004$ the radius of emerging bubbles is approximately equal to $R_C = 0.00004 \text{ m}$. Since the surface tension coefficient normalized using PDMS1000 density is $\chi = 0.02 \text{ m}^3\text{s}^{-2}$ at 20°C , the inertial force ratio at the location of the bubble to the surface tension force is approximately 1.26. Therefore, the influence of the surface tension force is significant here. As a result, existing DNS methods for cavitating flows without taking into account surface tension (as described in [24]) must be modified to account for the effect of surface tension.

Conclusion

Periodic chain of bubbles in flows between cylinders is described using the velocity potential for nonaxisymmetric perturbations of these flows. It is shown that the constant distance between two parallel axes of the cylinders leads to the appearance of undulating pressure distributions along them. Regular system of pressure minima leads to the appearance of the regular system of caverns with practically

constant distances between them. „The wavelength“ of the system is determined by the minimum clearance between the cylinders. Comparison of calculations with experimental data showed the ability of the developed calculation model to satisfactorily predict the azimuth and axial location of emerging caverns. So, it can be stated that the nature of the chain under study has been discovered. Although the described flow model does not make it possible to quantitatively predict the number of cavitation occurrence, the performed calculations allow to conclude that the deviation from the axisymmetric flow (the distance between the axis of the inner cylinder and the axis of the outer one) is more significant for the occurrence of cavitation than the increase in the rotation speed, and since these deviations are essentially three-dimensional, their influence cannot be analyzed using the Reynolds equation for lubrication.

Finally, it should be noted that the fluid flow models developed by Professor Stepanov (he would have turned 100 years old in 2022) remain effective for solving problems in the theory of cavitation.

Conflict of interest

The author declares that he has no conflict of interest.

References

- [1] A.A. Monakhov, V.M. Chernyavski, Y. Shtemler. *Phys. Fluids*, **25**, 093102 (2013).
- [2] A. Harnoy. *Bearing Design in Machinery* (Taylor & Francis. Bosa Roca, US, 2002)
- [3] V.R. Nosov, J. Gomez-Mancilla, J.A. Meda-Campana. *Water Sci. Techn.*, **64**, 593 (2011).
- [4] T. Tang, N. Morris, J. Coupland. *J. Physics: Conference Series*, **656**, 012119 (2015).
- [5] V. Shinde, N. Padawale, H. Tambat. *ARPN J. Eng. Appl. Sc.*, **11**, 7936 (2016).
- [6] Y. Song, X. Ren. *ASME J. Tribology*, **137**, 011701 (2015).
- [7] D.Y. Dhande, D.W. Pande. *J. King Saud University — Eng. Sc.*, **30**, 345 (2018).
- [8] P. Reinke, M. Schmidt, T. Beckmann. *Phys. Fluids*, **30**, 104101 (2018).
- [9] D. Dowson, C.M. Taylor. *Ann. Rev. Fluid Mech.*, **11**, 35 (1979).
- [10] M.J. Braun, W.M. Hannon. *Proceedings of the Inst. Mech. Eng., Part J: J. Eng. Tribology*, **224**, 839 (2010).
- [14] E.L. Amromin, S.I. Kovinskaya. *J. Fluids Structures*, **34**, 84 (2012).
- [12] E.L. Amromin. *Intern. J. Multiphase Flows*, **124**, 103188 (2020).
- [13] G. Korn, T. Korn. *Spravochnik po matematike* (Nauka, M., 1970) (in Russian)
- [14] E.L. Amromin, G.Yu. Stepanov, Yu.S. Timoshin. *ZhTF*, **65**(10), 13 (1995) (in Russian)
- [15] D. Batchelor. *Vvedeniye v dinamiku zhidkosti* (Mir, M., 1973) (in Russian)
- [16] E.L. Amromin. *MZhG Izvestiya AN SSSR*, **20**, 871 (1985).
- [17] G.Yu. Stepanov. *Izbrannyye voprosy sovremennoy mekhaniki* (IM MGU, 1982), p. 5.
- [18] O. Coutier-Delgosha, F. Deniset, J.A. Astolfi, J.-B. Leroux. *ASME J. Fluids Eng.*, **129**, 279 (2007).
- [19] L.V. Gogish, G.Yu. Stepanov. *Otryvnyye i kavitatsionnyye techeniya* (Nauka, M., 1990)
- [20] M.L. Billet, J.W. Holl. *ASME J. Fluids Eng.*, **103**, 405 (1981).
- [21] G.Yu. Stepanov. *Trudy MIAN*, **186**, 31 (1989) (in Russian)
- [22] S. Dabiri, W.A. Sirignano, D.D. Joseph. *Physics of Fluids*, **22**(4), 042102 (2010).
- [23] A.A. Monakhov, V.D. Kotelkin. *Izv. RAN. MZhG*, **3**, 81 (2017).
- [24] A. Znidarcic, O. Coutier-Delgosha, M. Marquillie, M. Dular. *J. Physics: Conf. Series*, **656**, 012143 (2017).